Supporting Information: On-chip Heaters for Tension Tuning of Graphene Nanodrums

D. Davidovikj[1‡],[1,*] M. Poot[1,2,3‡],[1,†] S. J. Cartamil-Bueno[1],[1]

H. S. J. van der Zant[1],[1] and P. G. Steeneken[1,41]

[11] *Kavli Institute of Nanoscience, Delft University of Technology, Lorentzweg 1, 2628 CJ Delft, The Netherlands*

[2] *Physik Department, Technische Universität München, D-85748 Garching, Germany*

[3] *Institute for Advanced Study, Universität München, 85748 Garching, Germany*

[4] *Department of Precision and Microsystems Engineering, Delft University of Technology, Mekelweg 2, 2628 CD, Delft, The Netherlands*

[*] d.davidovikj@tudelft.nl

[†] menno.poot@tum.de;

‡Authors contributed equally

Symbols

Used symbols (units):

V_{H}: heater voltage (V)

I_{H}: heater current (A)

R_{H}: heater resistance (Ω)

V_{off}: offset voltage (V)

I_{off}: offset current (A)

V_{meas}: measured voltage (V)

I_{meas}: measured current (A)

R_{meas}: measured resistance (Ω)

U_{el}: elastic energy (J)

F_{el}: restoring elastic force (N)

F_{es}: electrostatic force (N)

n_0: in-plane tension (N/m)

$n_0(0)$: pre-tension (N/m)

E: Young's modulus (Pa)

h: thickness (m)

z: displacement of the center of the membrane (m)

R: radius (m)

ν: Poisson's ratio

C: capacitance (Fa)

V_{G}: DC gate voltage (V)

A: area of drum (m^2)

g: gap size (m)

ε_0: dielectric constant

f_0: resonance frequency (Hz)

m: effective mass (kg)

k: effective stiffness (N/m)

α_{eff}: thermal expansion of the graphene-heater system (1/K)

κ: thermal conductivity of the silicon oxide (W/K)

I. Temperature profile simulations

In this section we lay out the details of the 3D finite-elements simulations of the temperature increase in the heater structure. In the simulations, we take a heat flux of 81 mW through the heater, while keeping the bottom of the silicon chip thermally anchored. In Fig. S1(a) we show the temperature across the cutline running horizontally through the heater structure. This is to estimate the influence of the heat conductance through the electrodes and bonding wires on the thermal profile of the heater, the simulation is repeated for a case where the edges of the heater are also thermally anchored. It is shown that in both cases the temperature at the center of the heater is the same (25 K), proving that heat transport through the leads is negligible and the dominant heat sink is the silicon through the thin layer of SiO_2.

To evaluate the dominant thermal resistance of the system, a vertical cutline through the Si-SiO_2-AuPd is shown in Fig. S1(b). The thermal profile along the z-axis shows that the thermal resistance of SiO_2 is dominant in the system, as the total temperature drop across the silicon is less than 1 K.

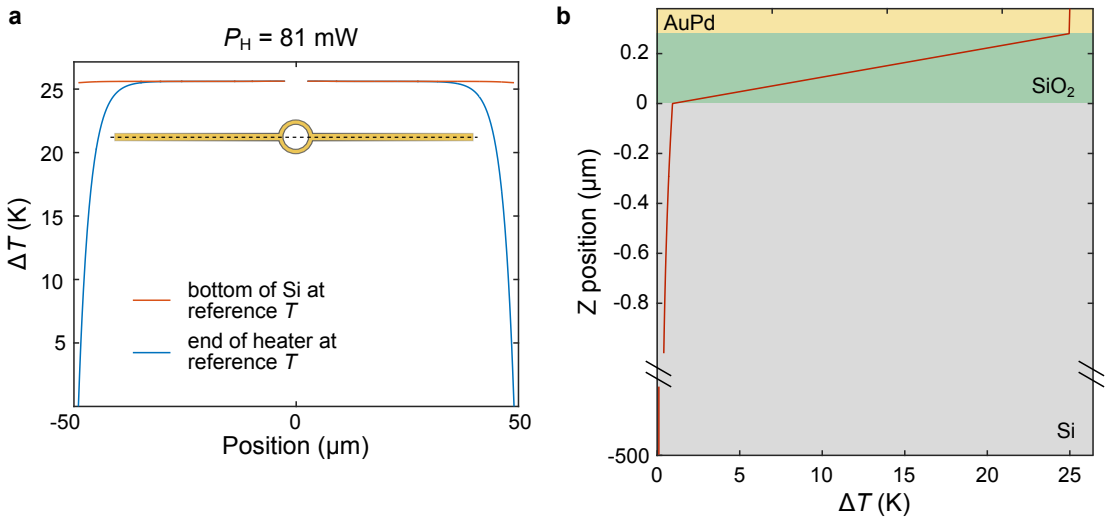

FIG. S1. Temperature profiles of the heater device. (a) Horizontal cutline through the heater device (dashed line in inset) for two cases: the red line is the temperature along the heater structure when the thermal reference (293 K) is at the bottom of the Si chip. The blue line shows the temperature profile when the thermal sink is at the edges of the heater electrodes, through the bonding wires. (b) Temperature profile along the vertical direction when the Si chip is at the reference temperature (293 K). Almost the entire temperature drop is across the SiO_2 layer.

II. Resistance measurement

In the experiments the resistance of the heater R_{H} is measured using a Keithley 2400 Sourcemeter. This is done by setting the desired voltage on the Sourcemeter and measuring both the actual heater voltage V_{H} as well as the current I_{H} that flows through it. Such monitoring is done during the mechanical measurements, as well as in separate characterization measurements where V_{H} is swept (cf. Fig. 1(e), main text). Naturally, the resistance is the ratio of the voltage to the current. However, the measured values can have offsets w.r.t. their true values: $V_{\mathrm{meas}} = V_{\mathrm{H}} + V_{\mathrm{off}}$ and $I_{\mathrm{meas}} = I_{\mathrm{H}} + I_{\mathrm{off}}$. This is illustrated

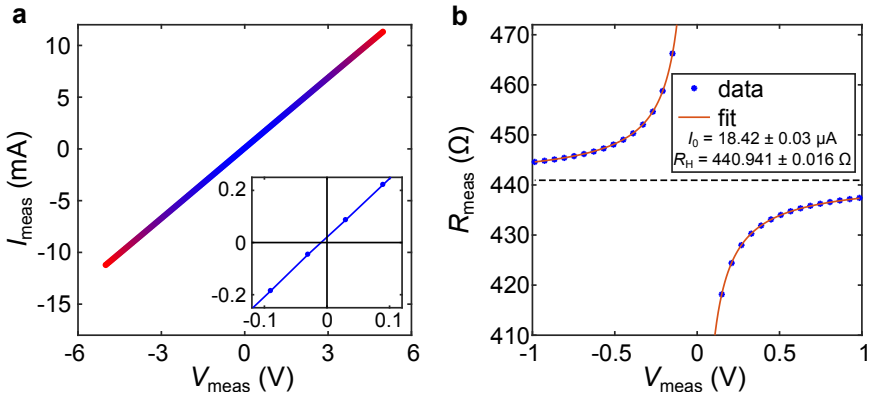

FIG. S2. (a) Heater current-voltage measurement. The inset shows a zoom of the data. (b) Measured resistance and fit of Eq. S1.

in Fig. S2(a) using the data from Fig. 1(d) from the main text. The IV curve does not go through the origin, indicating that current offsets, voltage offsets, or both, are present. When with these present, simply dividing the measured voltage and current does not give the right resistance R_{H}:

$$R_{\mathrm{meas}} = \frac{V_{\mathrm{meas}}}{I_{\mathrm{meas}}} = \frac{V_{\mathrm{H}} + V_{\mathrm{off}}}{I_{\mathrm{H}} + I_{\mathrm{off}}} = R_{\mathrm{H}} \times \frac{I_{\mathrm{H}} + V_{\mathrm{off}}/R_{\mathrm{H}}}{I_{\mathrm{H}} + I_{\mathrm{off}}} = R_{\mathrm{H}} \times \frac{V_{\mathrm{H}} + V_{\mathrm{off}}}{V_{\mathrm{H}}/R_{\mathrm{H}} + I_{\mathrm{off}}} \neq R_{\mathrm{H}}. \tag{S1}$$

In particular, Eq. S1 shows that the measured resistance approaches R_{H} for large I_{H}, but also that it diverges at $I_{\mathrm{H}} = -I_{\mathrm{off}}$.

Although Eq. S1 contains both V_{off} and I_{off}, these cannot be determined independently from a measurement of $R_{\mathrm{meas}}(V_{\mathrm{meas}})$ as Eq. S1 can be rewritten as:

$$R_{\mathrm{meas}}(V_{\mathrm{meas}}) = \frac{V_{\mathrm{meas}}}{V_{\mathrm{meas}}/R_{\mathrm{H}} + (I_{\mathrm{off}} - V_{\mathrm{off}}/R_{\mathrm{H}})}, \tag{S2}$$

after eliminating I_{meas}. This only contains the combination of I_{off} and V_{off} as a single parameter $I_0 \equiv I_{\mathrm{off}} - V_{\mathrm{off}}/R_{\mathrm{H}}$.

Figure S2(b) shows the measured resistance R_{meas} as well Eq. S2 fitted to the data. The model fits the data well, and gives the fit values for the combined offset $I_0 = 18.42\,\mu\mathrm{A}$ and the heater resistance $R_{\mathrm{H}} = 440.94\,\Omega$. Note that even at $V_{\mathrm{H}} = \pm 1\,\mathrm{V}$ the deviation between R_{meas} and R_{H} is significant, a few Ohm, especially compared to the changes that occur while changing the temperature or heater voltage as shown in Fig. 1(d). This offset is taken into account in the temperature dependence of Fig. 1(d) where the current is measured at $V_{\mathrm{H}} = -1\,\mathrm{V}$.

Finally, Eq. S1 can be inverted, giving:

$$R_{\mathrm{H}} = \frac{V_{\mathrm{meas}} - R_{\mathrm{H}}(I_{\mathrm{off}} - I_0)}{I_{\mathrm{meas}} - I_0} = \frac{V_{\mathrm{meas}}}{I_{\mathrm{meas}} - I_0}. \tag{S3}$$

For the last equality, the fact that $I_0 \equiv I_{\mathrm{off}} - V_{\mathrm{off}}/R_{\mathrm{H}}$ holds for every combination of I_{off} and V_{off} that gives the same I_0, including for $V_{\mathrm{off}} = 0$, is used. Now by fitting the low-voltage region [Fig. S2(b)] where R_{H} is practically constant, one obtains the fit value for I_0 that can be inserted into Eq. S3 to find the actual resistance R_{H} from the raw measurements. The results in Fig. 1(d) are obtained using this procedure.

III. Interplay between in-plane and out-of-plane tension

In this section, we outline the model for the influence of thermally-induced in-plane tension on the gate tunability of the resonance frequency of the membrane. The deformation of the drum under an electrostatic load is taken to be parabolic, such that its deformation shape is given by: $U(r) = 1 - \frac{r^2}{R^2}$, where R is the radius of the membrane. This is very close to the shape of the fundamental eigenmode $u(r, \phi) = J_0(kr), k \approx 2.404/R$.

The potential energy of a deformed membrane is mainly determined by the stretching energy. This is because for thin membranes we can neglect bending rigidity, provided that the condition $\frac{h^3}{d^2}\frac{E}{n_0} \ll 1$ is satisfied [1]. The potential energy of a spherically deformed membrane (by a uniform pressure load) is then given by:

$$U_{\mathrm{el}} = 2\pi n_0 z^2 + \frac{2\pi E h}{3R^2(1-\nu)} z^4, \tag{S4}$$

where z is the displacement of the center of the drum. The restoring force can be calculated as:

$$F_{\mathrm{el}} = \frac{dU_{\mathrm{el}}}{dz} = 4\pi n_0 z + \frac{8\pi E h}{3R^2(1-\nu)} z^3, \tag{S5}$$

To derive the electrostatic force felt by the drum, we make the parallel plate capacitor and the uniform electrostatic load approximations, which are valid for small deflections.

$$F_{\mathrm{es}} = \xi \frac{1}{2} \frac{\varepsilon_0 A}{(g-z)^2} V_{\mathrm{G}}^2, \tag{S6}$$

where ξ accounts for the projection of the force on the center of the membrane. For a parabolic deformation $\xi = 0.5$.

Expanding this around $z = 0$, we get:

$$F_{\mathrm{es}} = \frac{1}{4}\varepsilon_0 A V_{\mathrm{G}}^2 \left(\frac{1}{g^2} + \frac{2z}{g^3} + O(z^2) \right) \tag{S7}$$

We can now write the force-balance equation of the system:

$$F_{\mathrm{el}} - F_{\mathrm{es}} = 4\pi n_0 z + \frac{8\pi E h}{3R^2(1-\nu)} z^3 - \frac{1}{4}\varepsilon_0 A V_{\mathrm{G}}^2 \left(\frac{1}{g^2} + \frac{2z}{g^3} \right) = 0, \tag{S8}$$

which can be rewritten as:

$$\frac{8\pi Eh}{3R^2(1-\nu)}z^3 + \left(4\pi n_0 - \varepsilon_0 A V_{\mathrm{G}}^2 \frac{1}{2g^3}\right)z - \varepsilon_0 A V_{\mathrm{G}}^2 \frac{1}{4g^2} = 0. \tag{S9}$$

Equation S9 is then used to calculate the equilibrium position $z(V_{\mathrm{G}}, n_0)$ of the drum.

The effective stiffness of the system k is given by:

$$k = 4\pi n_0 - \frac{\varepsilon_0 A V_{\mathrm{G}}^2}{2g^3} + \frac{8\pi Eh}{R^2(1-\nu)}z^2, \tag{S10}$$

which is also close to the dynamic spring constant of the fundamental mode.

The resonance frequency of the membrane can then be estimated as:

$$f_0 = \frac{1}{2\pi}\sqrt{\frac{k}{m_{\mathrm{eff}}}}, \tag{S11}$$

where m_{eff} is the effective mass of the fundamental resonance mode ($m_{\mathrm{eff}} = \frac{1}{3}$m assuming parabolic deformation). The pre-tension of the drum is calculated from the resonance frequency at zero heater- and gate-voltage: $n_0(0) = 0.033$ N/m. By substituting for z from eq. S9 into eq. S10 and plugging this into eq. S11, we numerically calculate the resonance frequency as a function of the DC voltage for varying in-plane tension. Figure S3(a) shows the simulated f_0 vs. V_{G} curves for four different values of the in-plane tension together with polynomial fits, which is a good approximation provided that the tension-induced hardening is much stronger than the electrostatic softening, which seems to be the case judging by the measurements presented in the main text. The effective Young's modulus E is extracted from numerical fitting of the the blue data points in panel (a), for zero heater voltage.

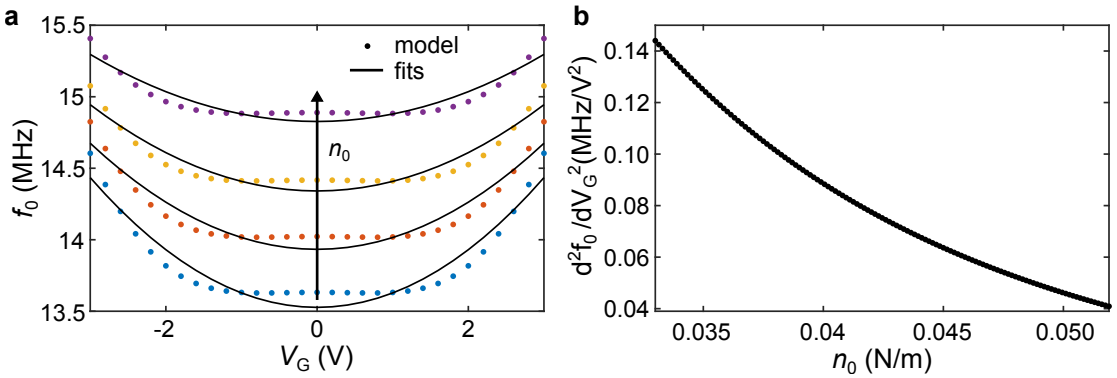

FIG. S3. (a) Modeled f_0 vs. V_{G} curves for increasing in-plane tension n_0 (colored data points) together with polynomial fits (black curves). (b) Extracted curvature from the polynomial fits of the curves shown in (a) as a function of the in-plane tension n_0.

Panel (b) of Fig. S3 shows the curvature at $V_{\mathrm{G}} = 0$ V as a function of the in-plane tension.

By relating the pre-tension to the heater voltage, we extract the thermal expansion coefficient of the system.

The relation between the heater-induced in-plane tension and V_{H} can be written as:

$$n_0 = n_0(0) + \Delta n_0(V_{\mathrm{H}}), \tag{S12}$$

where $n_0(0)$ is the pre-tension of the drum at room temperature and $\Delta n_0(V_{\mathrm{H}})$ is the added tension due to heating. The thermally induced tension $\Delta n_0(V_{\mathrm{H}})$ is related to the thermally added strain ϵ through:

$$\Delta n_0(V_{\mathrm{H}}) = \epsilon E h. \tag{S13}$$

The strain ϵ is, in turn, related to the thermal expansion of the system:

$$\Delta n_0(V_{\mathrm{H}}) = \alpha_{\mathrm{eff}} \Delta T E h. \tag{S14}$$

The temperature increase of the system at a given voltage is determined by the total heating power and the thermal conductivity of the system:

$$\Delta T = \frac{P_{\mathrm{H}}}{\kappa} = \frac{V_{\mathrm{H}}^2}{R_{\mathrm{H}} \kappa}, \tag{S15}$$

which yields:

$$n_0 = n_0(0) + \alpha_{\mathrm{eff}} E h \frac{V_{\mathrm{H}}^2}{R_{\mathrm{H}} \kappa}. \tag{S16}$$

The factor $\frac{1}{R_{\mathrm{H}} \kappa} = 0.72\,\mathrm{K/V^2}$ is experimentally determined from the temperature calibration of the heater shown in Fig. 1 of the main text. Since E is known from fitting the curve of Fig. S3(a), the pre-factor $\frac{Eh}{R_{\mathrm{H}} \kappa}$ is found to be $\frac{Eh}{R_{\mathrm{H}} \kappa} = 432\,\mathrm{NK/V^2 m}$.

We now use this relation to numerically fit the measured resonance frequency as a function of heater voltage to estimate α_{eff}. The net thermal expansion coefficient of the system is found to be: $\alpha_{\mathrm{eff}} = 1.64 \times 10^{-6}\,\mathrm{K^{-1}}$. Substituting this value in the expression for n_0 in Fig. S3 (b), we get a good agreement with the extracted curvature from Fig. 3 (e) of the main text.

IV. Other devices

In this section we present data on two other graphene devices. Similarly to Fig. 3 (g) from the main text, Fig. S4 shows $f_0 - Q$ plots for (a) a 5-nm thick and (b) a 18-nm thick graphene drum. Both drums show the same trend: upon increasing the heater voltage (i.e. the temperature of the heater), both the frequency and the quality factor go up. The thin drum (Fig, S4 (a)) shows a ≈30 % frequency increase accompanied by a 56 % increase in the quality factor. The 18-nm thick sample shows a minute frequency increase of 3 %, probably owing to the fact that the resonance of thicker drums is determined by their bending rigidity, rather than the tension. The quality factor, however, shows an increase of 121 %, which is a significant improvement of the mechanical dissipation.

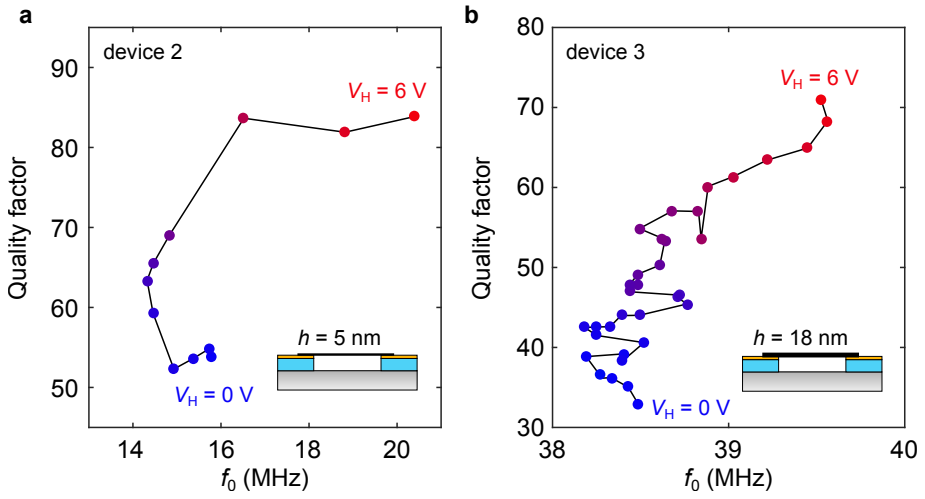

FIG. S4. Thermal tuning of two other graphene devices: (a) a 5-nm thick few-layer graphene and (b) a 18-nm ultra-thin graphite drum. The resonance frequency is plotted against the quality factor while heating the device up. The color of each dot corresponds to the temperature of the device.

V. Independent tuning of f_0 and Q

In this Section we demonstrate that we can independently tune the resonance frequency and the quality factor. Figure S5(a) shows the accessible range in the $f_0 - Q$ space, showing all the measurement curves of Fig. 3 from the main text. The area in gray represents the accessible $f_0 - Q$ space by using the dc heater and gate voltages, V_{H} and V_{G}, as control parameters. However, from this plot, as well as the data in Fig. 3, it is clear that when changing either $V_{\mathrm{G,eff}}$ or V_{H}, both the quality factor and the resonance frequency change simultaneously.

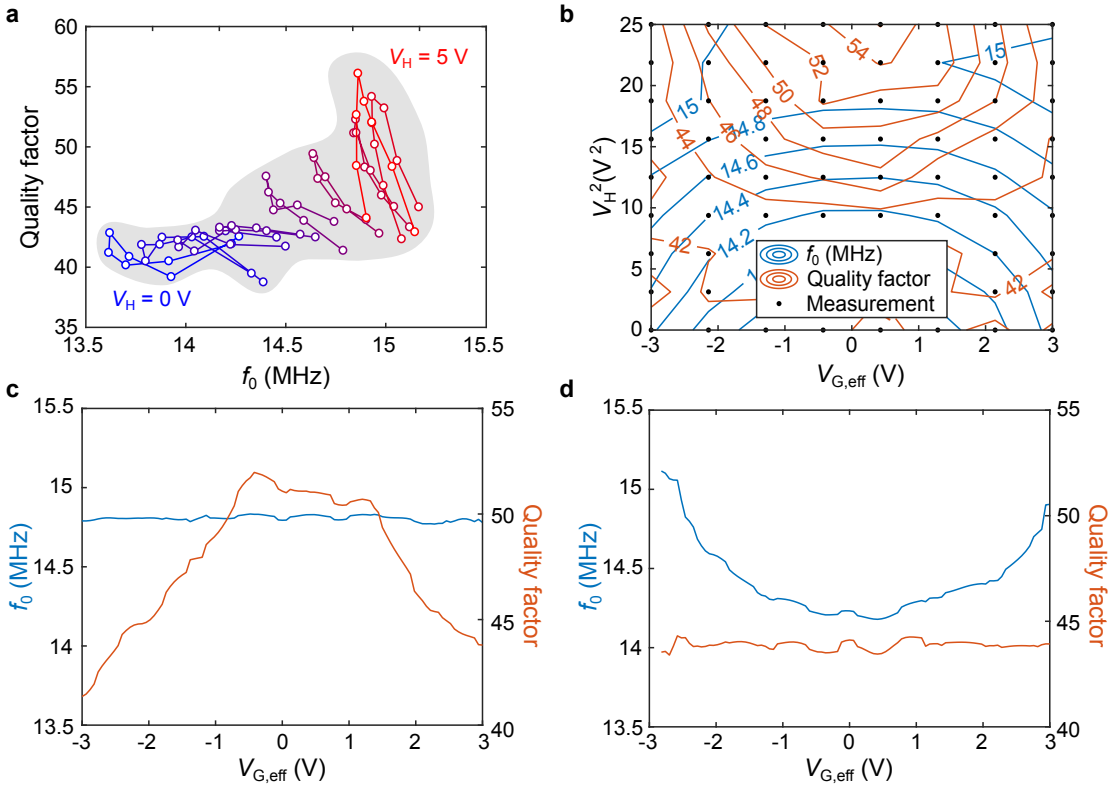

FIG. S5. (a) $f_0 - Q$ plot for varying heater and gate voltage. The gray area indicates the accessible region. Each color represents a different heater voltage. (b) A double contour plot of the resonance frequency and the quality factor for varying $V_{\mathrm{G,eff}}$ and V_{H}. Experimental values are measured at the locations of the black dots. Independent tuning of the (c) quality factor and (d) resonance frequency by following one of the contour lines of (b).

In Fig. S5(b) we visualize the same data using contour plots. These lines of constant f_0 and Q are calculated using the `contour` function of Matlab R2017a. The x-axis shows the

gate voltage $V_{\mathrm{G,eff}}$ and the y-axis is the (square of the) heater voltage V_{H}^2. The blue curves are lines of equal resonance frequency and the orange curves are lines of equal quality factor. By definition, when following a contour line of either f_0 or Q, the value of it remains constant. The fact that a single blue contour intersects more than one orange contour and vice versa shows that for a given value of one parameter, the other can be tuned independently in the range given by the outermost intersection points of the two curves. Using a combination of V_{H} and V_{G}, we can follow either contours of constant frequency or have constant quality factors, as shown in Fig. S5(c-d). In Fig. S5(c) we show that we can keep the resonance frequency constant (blue curve), while lowering the quality factor (orange curve). The opposite effect is observed in Fig. S5(d): where we follow a contour of constant Q, while the resonance frequency increases.

Technically, the contour curves are parameterized with the $V_{\mathrm{G,eff}}$ as control parameter and the corresponding value of V_{H}^2 is calculated from the output of the `contour` function using `interp1` with the `'pchip'` option. Next, for each point along the curve a 2D interpolation is performed to find the local values of f_0 and Q. Due to the difference in the interpolation algorithm and that in the `contour` function, small fluctuations in the "constant" parameter are still visible. However, the changes in the other, i.e, "varying" parameter is much larger. This clearly demonstrates the power of our system to have independent control over the resonance frequency and damping of the graphene nanodrum.

---

[1] Mansfield, E. H., The bending and stretching of plates. *Cambridge University Press*, Cambridge, UK, **2005**.